

# Catalysis Science & Technology

Accepted Manuscript

This article can be cited before page numbers have been issued, to do this please use: S. Zhang, J. Lee, D. H. Kim and T. J. KIM, *Catal. Sci. Technol.*, 2020, DOI: 10.1039/C9CY02619C.



This is an Accepted Manuscript, which has been through the Royal Society of Chemistry peer review process and has been accepted for publication.

Accepted Manuscripts are published online shortly after acceptance, before technical editing, formatting and proof reading. Using this free service, authors can make their results available to the community, in citable form, before we publish the edited article. We will replace this Accepted Manuscript with the edited and formatted Advance Article as soon as it is available.

You can find more information about Accepted Manuscripts in the [Information for Authors](#).

Please note that technical editing may introduce minor changes to the text and/or graphics, which may alter content. The journal's standard [Terms & Conditions](#) and the [Ethical guidelines](#) still apply. In no event shall the Royal Society of Chemistry be held responsible for any errors or omissions in this Accepted Manuscript or any consequences arising from the use of any information it contains.

## ARTICLE

**Effects of Ni Loading on the Physicochemical Properties of NiO<sub>x</sub>/CeO<sub>2</sub> Catalysts and Catalytic Activity for NO Reduction by CO**Shuhao Zhang <sup>a</sup>, Jaeha Lee <sup>b</sup>, Do Heui Kim <sup>b</sup> and Taejin Kim <sup>a†</sup>Received 00th January 20xx,  
Accepted 00th January 20xx

DOI: 10.1039/x0xx00000x

Transition metal oxide catalysts have been investigated extensively because of their relatively low costs and high activities in many chemical reactions. In this work, a series of NiO<sub>x</sub>/CeO<sub>2</sub> catalysts (0.5–30wt% Ni) were prepared using incipient wetness impregnation method. These catalysts were tested with various characterizations techniques, including Brunauer-Emmett-Teller (BET) theory, Raman spectroscopy, X-ray powder diffraction (XRD), Hydrogen Temperature-programmed reduction (H<sub>2</sub>-TPR) as well as Gas Chromatography (GC) for their physicochemical properties, surface properties, reduction properties and catalytic activities in the NO reduction by CO reaction. The increase in Ni loading of the catalyst (up to 5% NiO<sub>x</sub>/CeO<sub>2</sub>) led to decrease in specific surface area, formation of NiO<sub>x</sub> crystalline structures on CeO<sub>2</sub> surface, easier reduction of the catalyst comparing to bulk NiO<sub>x</sub> and bulk CeO<sub>2</sub>, as well as increase in catalytic activity in NO reduction by CO reaction. From these results, surface dispersion of NiO<sub>x</sub> and the formation of monolayer NiO<sub>x</sub> coverage of the catalysts were believed to affect the catalytic activities greatly. The results provided insights on the structure-activity relationship of NiO<sub>x</sub>/CeO<sub>2</sub> catalysts for NO reduction by CO reaction.

**Introduction**

Nitrogen oxides (NO<sub>x</sub>) are a leading pollutant source contributing to the increasing global environmental concerns and air pollutions.<sup>1</sup> One of the main sources of atmospheric NO<sub>x</sub> is anthropogenic activities like fuel combustion. During the past decades, many techniques, such as ammonia selective catalytic reduction (NH<sub>3</sub>-SCR) and NO reduction by hydrocarbon or CO, have been developed to catalytically reduce or eliminate NO<sub>x</sub> gases.<sup>2–4</sup> NO reduction by CO is among the most important approaches and has been adopted as one of the main reactions in the three-way catalytic converters (TWCs).<sup>5</sup> Thus, the NO reduction by CO reaction has been extensively investigated because two pollutants (NO and CO), which are both present in the automotive engine exhaust, can be converted into less polluted gases (N<sub>2</sub> and CO<sub>2</sub>) at the same time (2NO+2CO→N<sub>2</sub>+CO<sub>2</sub>).

Platinum group metals (PGM) have been applied to several NO<sub>x</sub> and CO removal procedures over the past decades.<sup>6–11</sup> However, due to the rarity, high prices of PGMs and their limitations in some catalytic reactions under lower reaction temperatures,<sup>12–14</sup> transition metal oxides have gained much attention as alternatives to PGMs. Nickel oxide is a promising candidate as it is one of the most reserved oxides on earth and

has excellent redox property.<sup>15,16</sup> Reddy et al.<sup>17</sup> reported that CuO-NiO/CeO<sub>2</sub>-Al<sub>2</sub>O<sub>3</sub> in CO oxidation reaction achieved 50% conversion at 364K and concluded that better dispersed and highly reducible metal oxides on the catalyst surface helped increasing catalytic activity. Atzori et al.<sup>18</sup> reported that NiO-CeO<sub>2</sub> mixed oxides prepared with both incipient wetness impregnation (IWI) and soft-templated method were very active and selective towards CO<sub>2</sub> methanation at mild conditions (400°C) after H<sub>2</sub> treatment because of the strong interactions between ceria support and the surface Ni<sup>0</sup> crystals, even though the Ni<sup>0</sup> crystals size were drastically different (~4nm for soft-templated catalyst and ~30nm for IWI catalyst). Ceria (CeO<sub>2</sub>) is a widely employed supporting material in heterogeneous catalyst systems as oxygen reservoir and thermal stabilizer.<sup>13,17</sup> Ceria is also known to be able to enhance the catalytic performance in ceria-containing catalysts.<sup>19–21</sup> Lee et al.<sup>22</sup> compared Pt/CeO<sub>2</sub> catalyst and Pt/γ-Al<sub>2</sub>O<sub>3</sub> catalyst and found that Pt dispersion in Pt/CeO<sub>2</sub> catalyst were much better after thermal treatment under 800°C because CeO<sub>2</sub> helped Pt species resisting sintering. Moreover, the authors noticed enhanced catalytic activity in CO oxidation reaction from Pt/CeO<sub>2</sub> catalyst prepared with 800°C pre-treated CeO<sub>2</sub>, due to the formation of PtO<sub>2</sub> on the catalyst surface and the weaker interaction between the surface PtO<sub>2</sub> and CeO<sub>2</sub> comparing to Pt metal and CeO<sub>2</sub>. He et al.<sup>23</sup> showed that CeO<sub>2</sub> modified Ni reached higher H<sub>2</sub> selectivity (99%) and higher turnover frequency value than that of bare Ni for hydrous hydrazine decomposition reaction. The addition of CeO<sub>2</sub> helped stabilizing the surface Ni species by forming a strong surface-support interaction as well as producing strong basic sites on the catalyst surface, which is beneficial for higher H<sub>2</sub> selectivity.

<sup>a</sup> Materials Science and Chemical Engineering Department, Stony Brook University, Stony Brook, NY, 11794, U.S.A

<sup>b</sup> School of Chemical and Biological Engineering, Institute of Chemical Processes, Seoul National University, Seoul 08826, Republic of Korea

† Corresponding Author: TJK: Materials Science and Chemical Engineering Department, Stony Brook University, Stony Brook, NY 11794, [tajejin.kim@stonybrook.edu](mailto:tajejin.kim@stonybrook.edu)

Moreover, NiO<sub>x</sub>/CeO<sub>2</sub> catalysts have shown promising results in NO reduction by CO. Wang et al.<sup>24</sup> synthesized ~7% NiO/CeO<sub>2</sub> catalyst with CeO<sub>2</sub> prepared from various methods (e.g. homogeneous precipitation and direct decomposition) and tested them in NO+CO and NO+CO+O<sub>2</sub> reactions. The authors found that, in NO/CO reaction, the NiO/CeO<sub>2</sub> catalyst reached ~100% NO conversion at ~200°C, whereas the NiO/γ-Al<sub>2</sub>O<sub>3</sub> catalyst reached ~100% NO conversion at 550°C and the NiO/TiO<sub>2</sub> catalyst showed maximum NO conversion of 80% at 600°C. The reason for higher catalytic activity in NiO/CeO<sub>2</sub> catalyst was attributed to the synergistic interaction between NiO and CeO<sub>2</sub> surface as evidence of easily reducible oxygen species were found on the NiO/CeO<sub>2</sub> catalyst surface. Cheng et al.<sup>25</sup> proposed a possible reaction mechanism of NiO/CeO<sub>2</sub> catalyst (7 wt% Ni loading) in NO reduction by CO via DRIFTS and mass spectroscopy (MS) studies. The authors suggested that, at 170°C, the NO+CO reaction happened in two steps: (1) CO reduction of surface oxygen; (2) NO dissociation on the reduced surface. These literatures' results provided some insight on the synthesis method effects as well as possible reaction mechanism of NiO<sub>x</sub>/CeO<sub>2</sub> catalysts in the NO+CO reaction at relatively low temperature (170°C). Although many literatures have highlighted the importance of NiO<sub>x</sub>/CeO<sub>2</sub> catalysts in the NO+CO reaction, NiO<sub>x</sub> loading effect was seldomly reported. In the present study, we investigated the effect of NiO<sub>x</sub> loading (0.5~30 wt%) on catalytic activity for the NO+CO reaction. The synthesized NiO<sub>x</sub>/CeO<sub>2</sub> catalysts were analyzed by BET, ICP-MS, XRD, Raman, and H<sub>2</sub>-TPR to understand the physicochemical properties and reducibility. Furthermore, to understand the intermediate species during the NO+CO reaction, in-situ diffuse reflectance infrared Fourier transform (DRIFT) spectroscopy was applied.

## Experimental

### Catalyst Synthesis

The ceria supported nickel oxide (NiO<sub>x</sub>) catalysts were synthesized by incipient wetness impregnation (IWI) method. First, desired amount of nickel (II) nitrate hexahydrate, 98% (Ni<sub>2</sub>NiO<sub>6</sub>·6H<sub>2</sub>O, from Alfa Aesar) were completely dissolved in ~0.5 mL de-ionized water to make Ni precursor solution. Then the precursor solution was added to ceria powder (HAS 5, from Rhodia) drop by drop while mixing constantly. After adding all the precursor solution, the mixture was dried at room temperature overnight and further dried at 120°C in a combustion boat with a tube furnace (Lindberg/Blue Mini-Mite, from Thermo). Finally, the catalyst was treated in air (100mL/min flow rate, Airgas, dry grade) atmosphere at 400°C (5°C/min ramping rate) for 6 hours to complete the calcination process and sieved (425 μm). The synthesized ceria supported nickel oxide catalysts are denoted as x% NiO<sub>x</sub>/CeO<sub>2</sub>, where x is the calculated Ni content during the synthesis process.

### Physical Property Measurement

The BET surface area and pore size distribution of the NiO<sub>x</sub>/CeO<sub>2</sub> catalysts were obtained by Micromeritics ASAP 2010. BET

method was used to calculate the specific surface area and BJH method was used to determine the pore size distribution of the catalysts. The tests were carried out at -196°C and N<sub>2</sub> was used for the adsorption/desorption process. The catalysts were treated at 300°C for 4 hours under vacuum to remove volatiles before the test.

The Ni content of the of the NiO<sub>x</sub>/CeO<sub>2</sub> catalysts were tested by ICP-MS technique. The samples were weighed and dissolved in aqua regia in a sealed Savillex teflon vial overnight on at hot plate at 110°C. The samples were then reconstituted in 2% nitric acid and diluted for Ni concentration analysis on an Agilent 7500cx quadrupole inductively-coupled plasma mass spectrometer. Samples were diluted to signal match mixed calibration standards and unknown concentrations were calculated based on standard calibration curves, with standards run frequently between unknowns to monitor drift in signal intensity.

### Powder X-ray Diffraction

Rigaku SmartLab diffractometer was used in the study to obtain Powder X-ray diffraction patterns of the NiO<sub>x</sub>/CeO<sub>2</sub> catalysts. The X-ray used was from Cu Kα radiation with wavelength of 0.1542 nm, voltage of 40 kV and current of 30 mA. The XRD patterns were collected from 10° to 90° with a frequency of 2.5°/min and step size of 0.02°.

### Raman Spectroscopy

In order to explore the molecular structures of NiO<sub>x</sub>/CeO<sub>2</sub> catalysts, Raman spectra of the dehydrated samples were obtained with visible (532 nm, BaySpec Nomadic™ Raman spectrometer) laser. The Raman spectrometer was equipped with a confocal microscope (Olympus BX-51 upright microscope), a dichroic filter, and Volume Phase Gratings (VPG). The visible laser excitation was generated by a diode-pumped solid-state continuous wave (DPSS CW). The visible 532nm Raman spectra were collected through a CCD detector (2048 x 64 pixels) in the 100-1400 cm<sup>-1</sup> Raman shift region. In order to collect the dehydrated catalyst Raman spectrum, the samples were placed in an *in-situ* environmental cell (Linkam CCR1000) and treated in 3% O<sub>2</sub>/Ar (Airgas) at 400°C for 1 hour. The Raman spectra of the dehydrated samples were collected after the samples were cooled down to room temperature. For each scan, the acquisition time was 30 seconds, and the final spectrum was accumulated from 10 scans.

### H<sub>2</sub>-TPR

BET-CAT-BASIC (from BEL Japan Inc.) with thermal conductivity detector (TCD) was used in this work for H<sub>2</sub>-TPR profile collections and data analyses. The catalysts were first treated in air atmosphere for 1 hour at 400°C for oxidation purposes, then cooled down to -90°C. After cooling down, 5% H<sub>2</sub> in Ar balance was introduced to initiate the reducing process. The temperature was then slowly increased from -90°C to 900°C (10°C/min) under reducing conditions for data collection.

### Catalytic Activity Tests and Stability Test

The NO reduction by CO reaction was carried out in a fixed bed quartz reactor (OD 9.6mm, ID 7mm) and quartz wool was used to make sure the position of the catalyst powder did not change. The reaction temperature was monitored with a K-type thermocouple which was in contact with the catalyst powder. The reaction temperature was increased from room temperature to 500°C with 1°C/min ramping rate. The reaction gases were made up of 5% NO (20 mL/min of 10% NO with He balance) and 5% CO (20 mL/min of 10% CO with He balance). Gas flow rate was monitored by FMA-1700 series mass flow meters and the space velocity was 31,200 h<sup>-1</sup>. Before the activity test, the catalyst powder (~40 mg) was pretreated in helium gas at 400°C for 30 min to remove impurities. The gas phase products were analyzed by TRACE™ 1300 GC (Thermo Scientific) containing a capillary column (Carboxen® 1010PLOT) and TCD detector. For the stability test, the reaction temperature was hold at 200°C for 12 hours and conversion data were collected every 30 min.

### In-situ DRIFTS Test

The *in-situ* DRIFTS results were obtained with Nicolet iS10 FT-IR (Thermo Scientific) with a Harrick Praying Mantis accessory cell. Similar to the activity test procedures, the catalyst was first pretreated at 400°C in Helium (40 mL/min) for 30 min to remove surface impurities and was then cooled down to room temperature. After the pretreatment, 5% NO (20 mL/min of 10% NO with He balance) and 5% CO (20 mL/min of 10% CO with He balance) were introduced to the sample holding cell. Before the collection of each spectrum, at least 25 min were allowed for the reaction to stabilize. Each spectrum was an average of 32 scans with 4 cm<sup>-1</sup> resolution for each scan.

## Results and Discussion

### Catalysts Characterization

#### Physical properties of catalysts

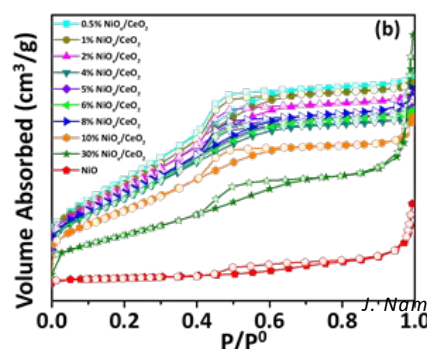
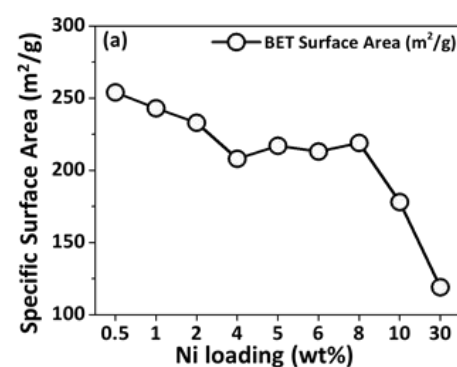
The Ni loading of the series of NiO<sub>x</sub>/CeO<sub>2</sub> catalysts were confirmed by ICP-MS tests and the results are shown in Table 1. The Ni wt% from the ICP-MS experimental data are very similar to the calculated Ni wt% (Calculated/ICP-MS ratio ≈ 1), indicating that the Ni loading on CeO<sub>2</sub> surface can be controlled by the incipient wetness impregnation method accordingly.

The specific surface area (SSA), N<sub>2</sub> adsorption-desorption isotherm, and pore size distribution of the series of NiO<sub>x</sub>/CeO<sub>2</sub> catalysts are shown in Figure 1. As the NiO<sub>x</sub> loading increased, the specific surface area of the catalyst decreased. It could be deduced that as Ni species was impregnated to the CeO<sub>2</sub> surface, some of the small pores could be blocked by the NiO<sub>x</sub>, resulting in a decrease in specific surface area. Also, the SSA of the NiO<sub>x</sub>/CeO<sub>2</sub> catalysts displayed a much more significant decrease when Ni loading was higher than 8%, possibly due to the formation of NiO crystalline structures, in addition to the blocking of small pores on CeO<sub>2</sub>. The N<sub>2</sub> adsorption-desorption isotherms of the NiO<sub>x</sub>/CeO<sub>2</sub> catalysts were typical type IV isotherms, indicating their mesoporous structures (Figure 1(b)).

Moreover, up to 10 wt%, the NiO<sub>x</sub>/CeO<sub>2</sub> catalysts displayed similar hysteresis loop shape, confirming that the pore structures of the NiO<sub>x</sub>/CeO<sub>2</sub> catalysts did not change much as Ni loading increased from 0.5 wt% to 10 wt%. The 30% NiO<sub>x</sub>/CeO<sub>2</sub> catalyst showed higher adsorption volume at  $\sim P/P^0 = 1$ , presumably due to the blocking of small pores and the retaining of larger pores. The pore size distribution results (Figure 1(c)) agreed with the previous findings. As it can be noticed, up to 10 wt%, the pore size distributions did not change much. The pore size distribution of 30% NiO<sub>x</sub>/CeO<sub>2</sub>, however, shifted to larger pore diameter, which was similar to the bulk NiO pore size distribution. From these results, it can be concluded that the pore structures of the NiO<sub>x</sub>/CeO<sub>2</sub> catalysts were not affected much by Ni loading up to 10% and the surface NiO<sub>x</sub> was relatively well dispersed without forming large crystalline NiO structure. For 30% NiO<sub>x</sub>/CeO<sub>2</sub>, crystalline NiO was formed on the surface of the catalyst, resulting in drastically different pore structures.

Table 1. Comparison between calculated Ni content and actual Ni content from ICP-MS

Calculated Ni wt %	Ni wt % from ICP-MS	Ni wt% Difference (ICP/calculated)
0 (bulk CeO <sub>2</sub> )	-	-
0.5	0.39	0.78
1	0.85	0.85
2	1.43	0.72
4	3.3	0.83
5	4.7	0.94
6	5.0	0.83
8	8.1	1.01
10	8.9	0.89
30	26.6	0.89



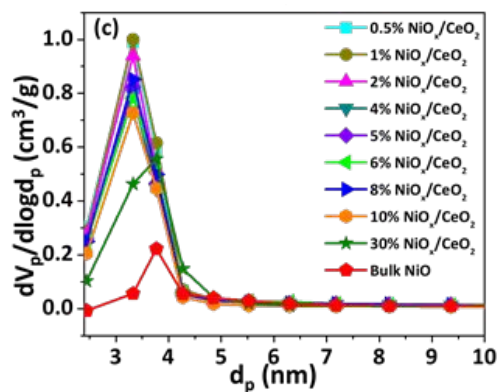


Figure 1. (a) BET surface area values of the  $\text{NiO}_x/\text{CeO}_2$  catalysts, (b)  $\text{N}_2$  adsorption-desorption isotherms of the  $\text{NiO}_x/\text{CeO}_2$  catalysts, and (c) pore size distribution of  $\text{NiO}_x/\text{CeO}_2$  catalysts

#### Powder X-ray Diffraction

To further investigate the crystalline structures of the  $\text{NiO}_x/\text{CeO}_2$  catalysts, powder X-ray diffraction (XRD) was used and the obtained XRD patterns of samples are shown in Figure 2. The XRD patterns of bulk  $\text{NiO}$  (1/10 scale) and bulk  $\text{CeO}_2$  were also included for reference. For the  $\text{NiO}_x/\text{CeO}_2$  catalysts, there were no obvious  $\text{NiO}$  patterns at  $37.5^\circ$  ( $\text{NiO}$  (111)) or  $43.5^\circ$  ( $\text{NiO}$  (200))<sup>28</sup> up to 6%  $\text{NiO}_x/\text{CeO}_2$ , while 8% and 10% samples' XRD pattern contained very weak  $37.5^\circ$  and  $43.5^\circ$  peaks (Figure 2 (b)). These two peaks became shaper as the Ni content increased to 30%, indicating the presence of larger  $\text{NiO}$  crystalline structures. Based on the XRD results, as the surface Ni loading increased, the surface  $\text{NiO}_x$  species were well dispersed up to 6%  $\text{NiO}_x/\text{CeO}_2$  and then started to form small crystalline  $\text{NiO}$  structures from 8%  $\text{NiO}_x/\text{CeO}_2$ . Furthermore, the increased surface  $\text{NiO}_x$  crystalline structures were expected in 10% and 30%  $\text{NiO}_x/\text{CeO}_2$  catalysts since they could lead to significant changes in physical properties (e.g., SSA and pore size) as shown in Figure 1 (a) and (c). In the case of the XRD patterns of  $\text{CeO}_2$  in the  $\text{NiO}_x/\text{CeO}_2$  samples, the prominent fluorite  $\text{CeO}_2$  peaks (fcc structure, PDF# 97-002-8709) at  $28.6^\circ$  (111),  $33.1^\circ$  (200),  $47.3^\circ$  (220) and  $56.3^\circ$  (311) were clearly present.<sup>29,30</sup> Moreover, the diffraction angles of the  $\text{CeO}_2$  peaks (e.g.  $28.6^\circ$ ) for all  $\text{NiO}_x/\text{CeO}_2$  samples were not shifted compared to bulk  $\text{CeO}_2$  (Figure 2 (c)). The intensity of the  $28.6^\circ$  peak was similar for all the  $\text{NiO}_x/\text{CeO}_2$  catalysts as well. The crystallite sizes of  $\text{CeO}_2$  in the series of  $\text{NiO}_x/\text{CeO}_2$  catalysts were calculated from the Scherrer equation (Eq. 1) and shown in Table 2.

$$D = 0.9\lambda / (B \cdot \cos\theta) \quad (\text{Eq. 1})$$

Where  $\lambda$  is the X-ray wavelength,  $B$  is the full width at half maximum (FWHM) of the  $\text{CeO}_2$  (111) peak, and  $\theta$  is the Bragg's angle of the peak.

As shown in Table 2, peak position of  $\text{CeO}_2$  (111) and average  $\text{CeO}_2$  crystallite size did not change much with different  $\text{NiO}_x$  loadings. It is worthwhile to note that the lattice parameter of  $\text{CeO}_2$  ( $\sim 5.41 \text{ \AA}$ ), which was calculated from the characteristic XRD peak of the  $\text{CeO}_2$  (111) peak by Bragg's law (Eq. 2), also remained unchanged after adding Ni species on the  $\text{CeO}_2$  surface.

$$\lambda = 2d_{111} \cdot \sin\theta_{111} \quad \text{and} \quad a = \sqrt{3}d_{111} \quad (\text{Eq. 2})$$

where  $\lambda$  is the wavelength of the incident wave ( $1.542 \text{ \AA}$ ),  $d$  is the spacing of lattice planes based on the corresponding peak position (111),  $\vartheta$  is the reflection angle based on the corresponding (111) peak position, and  $a$  is the lattice parameter.

The obtained results provided that the crystallite size as well as lattice structures of  $\text{CeO}_2$  were not affected by the addition of  $\text{NiO}_x$  species. It has been reported that the crystallite sizes of the solid solutions should be different comparing to bulk  $\text{CeO}_2$  due to the introduction of second metal cation into the  $\text{CeO}_2$  structure.<sup>31-34</sup> Based on the lattice parameter and crystallite size values, we expect that  $\text{Ni}^{2+}$  did not substitute  $\text{Ce}^{4+}$  in the  $\text{CeO}_2$  structure and solid solutions (e.g.  $\text{CeNiO}_x$ ) did not form in the  $\text{NiO}_x/\text{CeO}_2$  samples. Although XRD results provided crystalline structure information of  $\text{NiO}_x/\text{CeO}_2$  samples, the possibility of the presence of  $\text{NiO}_x$  nanocrystalline ( $< \sim 5 \text{ nm}$  particle size) structures on the  $\text{CeO}_2$  surface could not be completely ruled out due to the limitation of lab-scale XRD technique. Recently, Peck et al<sup>35</sup> and our group<sup>36</sup> reported that Raman spectroscopy could identify nanocrystalline structures in addition to determining the monolayer coverage of the  $\text{CeO}_2$  supported  $\text{MO}_x$  ( $M = \text{Fe}$  or  $\text{Co}$ ) catalysts. Thus, we then utilized Raman spectroscopy to study the  $\text{NiO}_x/\text{CeO}_2$  catalysts for further understanding of the molecular structures.

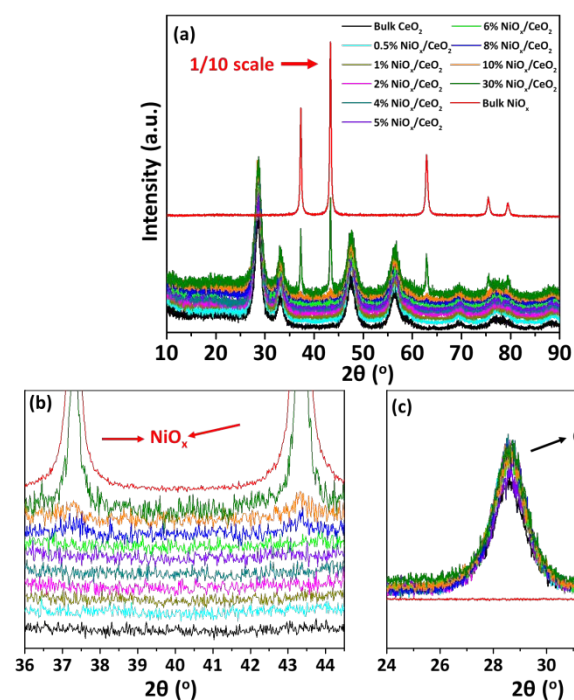


**Figure 2.** (a) Full range XRD patterns of NiO<sub>x</sub>/CeO<sub>2</sub> catalysts, (b) NiO<sub>x</sub> patterns region of NiO<sub>x</sub>/CeO<sub>2</sub> catalysts, and (c) CeO<sub>2</sub> patterns region of NiO<sub>x</sub>/CeO<sub>2</sub> catalysts

**Table 2.** CeO<sub>2</sub> crystallite sizes of NiO<sub>x</sub>/CeO<sub>2</sub> catalysts calculated from the XRD patterns

Calculated Ni wt %	FWHM of CeO <sub>2</sub> (111) peak (°)	Position of CeO <sub>2</sub> (111) peak (°)	Average CeO <sub>2</sub> crystallite size (nm)
0 (bulk CeO <sub>2</sub> )	1.358	28.59	6.31
0.5	1.306	28.59	6.56
1	1.327	28.63	6.46
2	1.327	28.61	6.46
4	1.363	28.55	6.29
5	1.413	28.63	6.06
6	1.441	28.65	5.95
8	1.280	28.61	6.69
10	1.386	28.63	6.18
30	1.370	28.61	6.25

### Raman Spectroscopy

As explained previously, Raman spectroscopy technique is widely used to obtain surface structure information of metal oxide and composite materials. The Raman spectra (532 nm) of the dehydrated NiO<sub>x</sub>/CeO<sub>2</sub> catalysts as well as bulk CeO<sub>2</sub> and NiO are presented in Figure 3. The bulk CeO<sub>2</sub> spectrum contained a sharp band at ~460 cm<sup>-1</sup> that corresponded to the F<sub>2g</sub> symmetric Ce-O-Ce vibrational mode of the fluorite structure of CeO<sub>2</sub>.<sup>35–38</sup> Other weak bands at ~236 cm<sup>-1</sup>, ~584 cm<sup>-1</sup> and ~1034 cm<sup>-1</sup> were ascribed to second-order transverse acoustic (2TA), defect-induced (D) and second-order longitudinal optical (2LO) mode vibrations, respectively.<sup>18,39,40</sup> Bulk NiO Raman spectra exhibited weak and broad bands at ~540 cm<sup>-1</sup>, ~760 cm<sup>-1</sup>, and ~1070 cm<sup>-1</sup>, which could be assigned

to longitudinal optic (LO) phonon mode, transverse optical two-phonon (2TO) modes, and second order scattering (2LO) mode vibrations, respectively.<sup>41–44</sup> In the case of NiO<sub>x</sub>/CeO<sub>2</sub> samples' Raman spectra, the CeO<sub>2</sub> F<sub>2g</sub> band (~460 cm<sup>-1</sup>) was observed up to 6 wt% NiO<sub>x</sub>/CeO<sub>2</sub> samples, and peak intensity continuously decreased with increasing Ni loading.

It could also be noticed that, in the 1000 cm<sup>-1</sup> to 1100 cm<sup>-1</sup> Raman shift regions, ~1070 cm<sup>-1</sup> band (bulk NiO, 2LO mode) was not observed under 4% NiO<sub>x</sub>/CeO<sub>2</sub>, while the more dominant peak was ~1034 cm<sup>-1</sup> peak (bulk CeO<sub>2</sub>, 2LO mode). After Ni loading reached 5%, the ~1070 cm<sup>-1</sup> peak became visible. Based on the Raman spectroscopy results, the surface NiO<sub>x</sub> monolayer could be formed between 4~5% Ni loading, even though XRD patterns did not have NiO peak up to 6 wt% NiO<sub>x</sub>/CeO<sub>2</sub> sample.

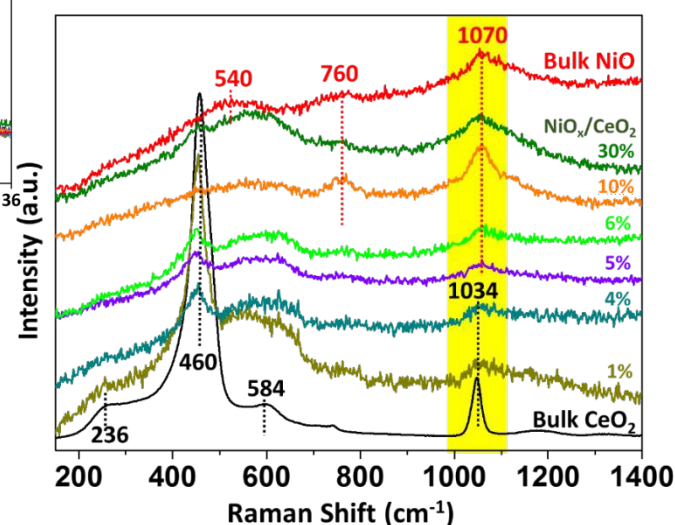


**Figure 3.** Raman spectra of the dehydrated NiO<sub>x</sub>/CeO<sub>2</sub> catalysts

### H<sub>2</sub> Temperature Programmed Reduction

In order to investigate the reduction properties of the NiO<sub>x</sub>/CeO<sub>2</sub> catalysts, H<sub>2</sub>-TPR tests were applied and the results are shown in Figure 4. The H<sub>2</sub>-TPR profiles of bulk NiO<sub>x</sub> (1/2 scale) was also included for reference. The bulk NiO<sub>x</sub> catalysts displayed a main peak at ~440°C as well as a shoulder peak at ~524°C. These two peaks could be assigned to the reduction of Ni<sup>2+</sup> → Ni<sup>δ+</sup> → Ni<sup>0</sup> in large crystalline structures of NiO<sub>x</sub>.<sup>45,46</sup> All the NiO<sub>x</sub>/CeO<sub>2</sub> catalysts showed a broad reduction peak at ~850°C, which corresponded to the reduction of bulk CeO<sub>2</sub>.<sup>47</sup> In the case of 0.5~5 wt% NiO<sub>x</sub>/CeO<sub>2</sub> catalysts (Figure 4 (a)), two reduction peaks were observed at < 500°C and these peaks were attributed to the reduction of well dispersed NiO<sub>x</sub> and surface CeO<sub>2</sub>.<sup>40,48</sup> As shown in Table 3, for example, the H<sub>2</sub> consumed for surface reduction of the 0.5 NiO<sub>x</sub>/CeO<sub>2</sub> catalyst was 0.9 mmol/g, whereas the surface Ni content was only 0.09 mmol/g. This result indicated that NiO<sub>x</sub> species and CeO<sub>2</sub> species were reduced simultaneously during the reduction of the catalyst surface. Moreover, for NiO<sub>x</sub>/CeO<sub>2</sub> catalysts with low Ni loading (especially <4 wt%), the overlapping of reduction peaks could be noticed in the TPR profiles, which was also in agreement with the simultaneous reduction of surface NiO<sub>x</sub> and CeO<sub>2</sub>. Also, according to literatures,<sup>47,49,50</sup> the reduction peaks

of surface oxygen on CeO<sub>2</sub> were often observed at 450~550°C. The well-dispersed surface NiO<sub>x</sub> improved the reducibility of CeO<sub>2</sub> surface. Many literatures have explained the promotion of the reducibility of CeO<sub>2</sub> surface by transition metals with H<sub>2</sub> spillover mechanism; <sup>51,52</sup> once NiO cluster is reduced to metallic Ni cluster, it would activate H<sub>2</sub> and spillover H atoms to reduce CeO<sub>2</sub> surface. However, there is also the alternative explanation, so called O<sub>2</sub> spillover mechanism, where the mobile O on CeO<sub>2</sub> surface could spill over to metallic Ni clusters to remove H<sub>2</sub> activated on the surface. <sup>53–55</sup> We believe that both spillover mechanisms would contribute to the improved reducibility of Ni/CeO<sub>2</sub> surface compared to CeO<sub>2</sub> surface. As shown in Figure 4 (a), as the NiO<sub>x</sub> loading increased from 0.5% to 5%, a clear shift of reduction temperatures was noticed. To be specific, the reduction peak of surface NiO<sub>x</sub> and CeO<sub>2</sub> gradually shifted from 307°C/379°C (0.5% NiO<sub>x</sub>/CeO<sub>2</sub>) to 158°C/253°C (5% NiO<sub>x</sub>/CeO<sub>2</sub>). These results indicated that, as the surface NiO<sub>x</sub> species increased (up to 5% NiO<sub>x</sub>/CeO<sub>2</sub>), the reducibility of the NiO<sub>x</sub>/CeO<sub>2</sub> catalysts were enhanced due to the synergistic relationship between NiO<sub>x</sub> and CeO<sub>2</sub>.<sup>56</sup> It is also interesting that highly dispersed NiO<sub>x</sub> complexes were reduced at lower temperature than bulk NiO<sub>x</sub>. The opposite behavior was often observed in other catalyst systems. For example, Pt or Pd species that are highly dispersed on CeO<sub>2</sub> surface have been reported to be reduced at higher temperature than their bulk counterparts (bulk PdO or bulk PtO<sub>2</sub>).<sup>57</sup>

For the 5%~30% NiO<sub>x</sub>/CeO<sub>2</sub> catalysts (Figure 4 (b)), the low temperature (<300°C) NiO<sub>x</sub> reduction temperatures stayed similar even as the Ni loading kept increasing. It is also worth pointing out that, starting from 6% NiO<sub>x</sub>/CeO<sub>2</sub>, the reduction peak for bulk NiO<sub>x</sub> at ~310°C could be observed. This trend indicated that the ~5% sample contained monolayer coverage of NiO<sub>x</sub> on CeO<sub>2</sub> surface, where the surface NiO<sub>x</sub> was well dispersed without NiO<sub>x</sub> crystalline structure formation. As the Ni content kept increasing, this peak became more defined and shifted to higher temperature (~310°C → ~397°C) in addition to the increase of H<sub>2</sub> consumptions. The difference between the surface Ni content and the H<sub>2</sub> consumption for surface reduction (Table 3) also decreased as the Ni loading increased, indicating that the NiO<sub>x</sub> species were covering the surface of the catalyst and less CeO<sub>2</sub> were exposed for surface reduction. For example, for the 30% NiO<sub>x</sub>/CeO<sub>2</sub> catalyst, the H<sub>2</sub> consumed to reduce catalyst surface was 5.13 mmol/g and the Ni content was 5.11 mmol/g. This result suggested that, for the 30% NiO<sub>x</sub>/CeO<sub>2</sub> catalyst, most of the exposed surface species was NiO<sub>x</sub> instead of CeO<sub>2</sub>, which agreed with the NiO<sub>x</sub> large crystalline structures identified in 30% NiO<sub>x</sub>/CeO<sub>2</sub> catalyst from XRD and Raman results.

So far, based on BET, Raman, XRD, and H<sub>2</sub>-TPR results, it could be concluded that, the addition of NiO<sub>x</sub> to CeO<sub>2</sub> greatly affected the physicochemical properties of the NiO<sub>x</sub>/CeO<sub>2</sub> catalysts (lower SSA, larger average pore size, formation of large NiO<sub>x</sub> crystalline structures, and enhanced reducibility comparing to bulk NiO<sub>x</sub>). The obtained results also provided that the monolayer coverage sample would be ~5% NiO<sub>x</sub>/CeO<sub>2</sub> and large NiO<sub>x</sub> (or bulk-like NiO<sub>x</sub>) crystalline structures were formed at > 10% NiO<sub>x</sub>/CeO<sub>2</sub>.

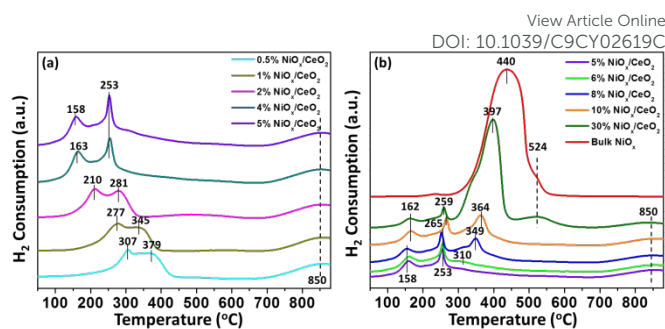


**Figure 4.** (a) H<sub>2</sub>-TPR profiles of NiO<sub>x</sub>/CeO<sub>2</sub> catalysts with Ni loading up to 5%, and (b) H<sub>2</sub>-TPR profiles of NiO<sub>x</sub>/CeO<sub>2</sub> catalysts with Ni loading higher than 5%

**Table 3.** Surface Ni content and H<sub>2</sub> consumption for surface reduction for the NiO<sub>x</sub>/CeO<sub>2</sub> catalysts

Calculated Ni loading (wt%)	Ni content calculated from Ni loading (mmol/g)	H <sub>2</sub> consumption for surface reduction (mmol/g)	Difference between surface H <sub>2</sub> consumption and Ni content (mmol/g)
0.5	0.09	0.90	0.81
1	0.17	0.92	0.75
2	0.34	0.95	0.61
4	0.68	1.28	0.6
5	0.85	1.37	0.52
6	1.02	1.46	0.44
8	1.36	1.80	0.44
10	1.70	2.09	0.39
30	5.11	5.13	0.02

### Catalytic Activity Test, Stability Tests and Space Velocity Effects

The catalytic activity test results of NiO<sub>x</sub>/CeO<sub>2</sub> catalysts for the NO reduction by CO reaction are shown in Figure 5. Overall, both NO and CO conversion increased with increasing temperature. Comparing to bulk NiO<sub>x</sub> and bulk CeO<sub>2</sub> catalysts, the supported NiO<sub>x</sub>/CeO<sub>2</sub> catalysts showed higher NO and CO conversion at lower reaction temperature, especially <300°C. It could be noticed that, although the Ni loading kept increasing, the NO conversions of the catalysts were similar after Ni loading reached 4~5%. Considering the previous discussions regarding mono-layer coverage of surface NiO<sub>x</sub>, it could be hypothesized that, when the surface NiO<sub>x</sub> loading was above monolayer, adding more Ni species was unlikely to keep improving the catalytic activity. Moreover, as presented in Figure 6, when the Ni loading increased from 0.5 to 4 wt%, the temperatures of NiO<sub>x</sub>/CeO<sub>2</sub> surface reductions and the T<sub>50</sub> of NO+CO reaction all decreased. For example, comparing 0.5% NiO<sub>x</sub>/CeO<sub>2</sub> and 4% NiO<sub>x</sub>/CeO<sub>2</sub> catalysts, the surface reduction starting temperature were 307°C and 163°C, T<sub>50</sub> of NO conversion were 227°C and

174°C, and  $T_{50}$  of CO conversion were 267°C and 186°C, respectively. Therefore, the highly dispersed  $\text{NiO}_x$  may have contributed to the catalytic activity. On the other hand, increasing Ni loading above 4-5 wt% did not decrease  $T_{50}$  further. From the XRD, Raman and  $\text{H}_2$ -TPR results, the formation of bulk  $\text{NiO}_x$  at high Ni loading (> 6 wt%) were observed. Therefore, bulk  $\text{NiO}_x$  may have low intrinsic activity in the NO-CO reaction and did not contribute to the catalytic activity in low reaction temperatures. Another finding worth pointing out is that, the  $T_{50}$  for supported  $\text{NiO}_x/\text{CeO}_2$  catalysts were much lower than those of bulk  $\text{NiO}_x$  and bulk  $\text{CeO}_2$ . This result confirmed the key role of  $\text{NiO}_x$  species on  $\text{CeO}_2$  in order to promote catalytic activity in NO reduction by CO reaction, as well as the synergistic effects between  $\text{NiO}_x$  and  $\text{CeO}_2$ . Furthermore, for the  $\text{NiO}_x/\text{CeO}_2$  catalysts, the NO conversion was higher than CO conversion at >150°C, and the difference became smaller as reaction temperature increased. The reason for the difference between NO and CO conversion could be explained by the reaction process. The NO reduction by CO reaction is considered to be a two-step reaction: (1) NO reduction into  $\text{N}_2\text{O}$  ( $2\text{NO} + \text{CO} \rightarrow \text{N}_2\text{O} + \text{CO}_2$ ), and (2)  $\text{N}_2\text{O}$  decomposition into  $\text{N}_2$  ( $\text{N}_2\text{O} + \text{CO} \rightarrow \text{N}_2 + \text{CO}_2$ ).<sup>33,58,59</sup> At lower reaction temperature (e.g. 150~250°C), the first step could be dominant, and the consumption ratio of NO/CO is ~2 if reacted stoichiometrically. The  $\text{N}_2$  selectivity and  $\text{N}_2\text{O}$  selectivity results (Figure 5 (c) and 5 (d)) also supported the two-step reaction mechanism as the selectivity was depended on the Ni loading and reaction temperature. This result indicated that, when the reaction temperature was < 250°C,  $\text{N}_2\text{O}$  was the dominant product. As reaction temperature increased further, the formed  $\text{N}_2\text{O}$  started to decompose, or NO was directly converted into  $\text{N}_2$  by CO ( $2\text{NO} + 2\text{CO} \rightarrow \text{N}_2 + 2\text{CO}_2$ ) without  $\text{N}_2\text{O}$  formation, resulting in the increase in  $\text{N}_2$  selectivity.

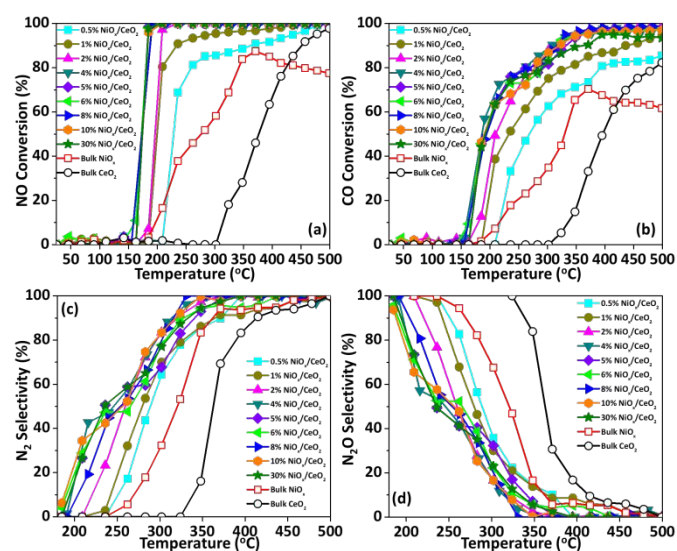


**Figure 5.** Catalytic activity of  $\text{NiO}_x/\text{CeO}_2$  catalysts in NO reduction by CO reaction. (a) NO conversion under different reaction temperatures, (b) CO conversion under different reaction temperatures, (c)  $\text{N}_2$  selectivity under different reaction temperatures, and (d)  $\text{N}_2\text{O}$  selectivity under different reaction temperatures.

Reaction conditions: 5% NO, 5% CO, balanced with Helium. ~40mg of catalyst was used. Total flow rate was 40mL/min.

DOI: 10.1039/C9CY02619C

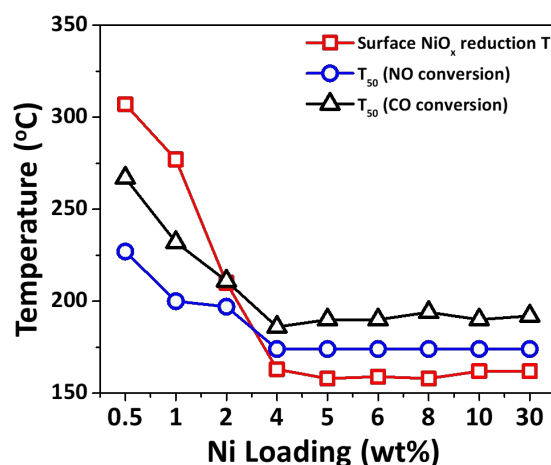


**Figure 6.** Surface reduction temperature of  $\text{NiO}_x/\text{CeO}_2$  catalysts,  $T_{50}$  of NO conversion and  $T_{50}$  of CO conversion of  $\text{NiO}_x/\text{CeO}_2$  catalysts in NO+CO reaction with different Ni loading

The stability test (time-on-stream test) was carried out on the 5%  $\text{NiO}_x/\text{CeO}_2$  catalyst which displayed good catalytic activity and  $\text{N}_2$  selectivity as shown in Figure 5. Overall, the 5%  $\text{NiO}_x/\text{CeO}_2$  catalyst did not show any severe deactivation during the 12-hour period of stability test under 200°C (Figure 7). The reason was probably that, since  $\text{CeO}_2$  performed as an oxygen reservoir, the redox cycle between  $\text{CeO}_2$  and surface  $\text{NiO}_x$  could quickly replenish surface oxygen whenever it was used or taken.

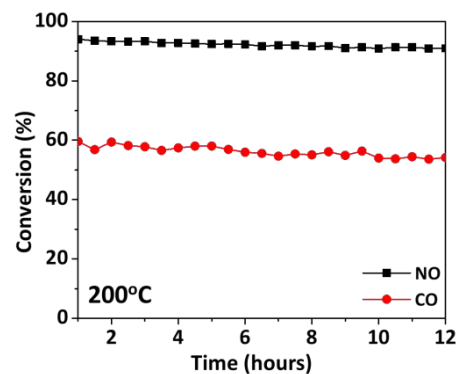


**Figure 7.** Time on stream results of 5%  $\text{NiO}_x/\text{CeO}_2$  in NO reduction by CO reaction at 200°C. Reaction conditions: 5% NO, 5% CO, balanced with Helium. ~40mg of catalyst was used. Total flow rate was 40mL/min.

To investigate the effect of internal diffusion resistances on the NO reduction by CO reaction over the  $\text{NO}_x/\text{CeO}_2$  catalyst, the different GHSVs (31,000  $\text{h}^{-1}$ , 7,000  $\text{h}^{-1}$ , and 124,000  $\text{h}^{-1}$ ) were applied to the 5%  $\text{NiO}_x/\text{CeO}_2$  catalyst under the same reaction temperature range. As shown in Figure 8, it is obvious that, within the tested reaction temperature range (25°C-500°C), the NO and CO conversion as well as  $\text{N}_2$  selectivity were very similar under different gas flow rates. Based on observed results, we can reasonably conclude that the NO reduction by CO reaction

over tested NiO<sub>x</sub>/CeO<sub>2</sub> catalyst should be free from the internal diffusion resistances under the current experimental conditions.

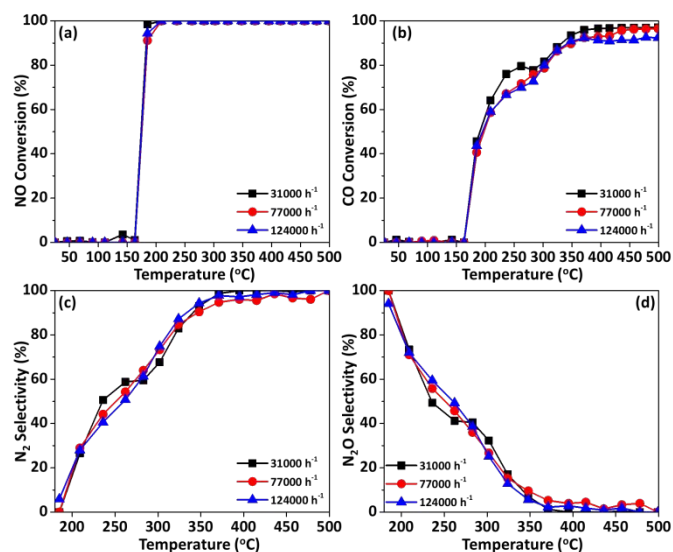


**Figure 8.** Catalytic activity of 5% NiO<sub>x</sub>/CeO<sub>2</sub> catalyst in NO reduction by CO reaction with various GHSV. (a) NO conversion under different reaction temperatures and GHSV, (b) CO conversion under different reaction temperatures and GHSV, (c) N<sub>2</sub> selectivity under different reaction temperatures and GHSV, and (d) N<sub>2</sub>O selectivity under different reaction temperatures and GHSV. Reaction conditions: 5% NO, 5% CO, balanced with Helium.

### *In-situ* DRIFTS Test

The specific reaction mechanism over supported transition metal oxide catalysts during NO reduction by CO reaction has been discussed a lot,<sup>14,33,59,60</sup> but detailed intermediate species and reaction mechanism are still under debate. In the current work, *in-situ* DRIFTS technique was applied to the 5% NiO<sub>x</sub>/CeO<sub>2</sub> catalyst in NO reduction by CO reaction to get more insights on the intermediate species as well as to explore the possible reaction mechanism. As shown in Figure 9 (a), at 50°C, several intermediate species could be identified: 1007 cm<sup>-1</sup> (bridging bidentate nitrate, O-N-O symmetric vibration), 1240 cm<sup>-1</sup> (bidentate nitrate), 1270 cm<sup>-1</sup> (monodentate nitrate), 1535 cm<sup>-1</sup> (monodentate nitrate), and 1593~1608 cm<sup>-1</sup> (bridging bidentate nitrate, N=O stretching).<sup>33,61-63</sup> As the reaction temperature increased up to 170°C, the nitrate intermediate species were still present, but the band intensity of 1593~1608 cm<sup>-1</sup> slowly decreased. According to the gas phase catalytic activity results (Figure 5 (a)), NO conversions were very low when the reaction temperature was under 170°C, indicating that nitrate intermediate species were stable on the catalyst surface. At 180°C, the adsorbed nitrate disappeared and a new band was observed at 1214 cm<sup>-1</sup>, which was attributed to the nitrite structures.<sup>31</sup> Note that the nitrite band was mainly observed between 180°C and 200°C, which was well matched to the N<sub>2</sub>O formation temperature as shown in Figure 9 (b). This result indicated that surface nitrite species should be the key intermediate species to form N<sub>2</sub>O. Also, this was the temperature range where N<sub>2</sub>O was the major product from the reaction as N<sub>2</sub> selectivity was lower than 50% (Figure 5 (c)).

Intermediate species involving CO were also observed in the spectra at 180°C. The 860 cm<sup>-1</sup>, 1358~1370 cm<sup>-1</sup>, and 1465 cm<sup>-1</sup> bands could be assigned to CO adsorption on the catalyst surface, symmetric vibration of monodentate carbonate, and bidentate carbonate, respectively.<sup>63-65</sup> At > 250°C, new bands appeared at 1465 cm<sup>-1</sup> and 1612 cm<sup>-1</sup> and the two bands could be assigned to the bidentate carbonate species.<sup>66,67</sup> The *in-situ* DRIFTS results clearly explained that the adsorption temperature of CO-related intermediate species (e.g. carbonate) was higher than the NO adsorption intermediate species (e.g. nitrate or nitrite). This result also indicated a possibility that, at lower reaction temperatures, NO intermediate species inhibited the access of CO to the catalyst surface.

Figure 9(b) displayed the bands representing the gas phase components. The gas phase NO band (~1870 cm<sup>-1</sup>) disappeared at > 180°C, matching well with the activity test where the 5% NiO<sub>x</sub>/CeO<sub>2</sub> catalyst showed >90% NO conversion at > 180°C. The gas phase CO band (~2150 cm<sup>-1</sup>) was also observed and the intensity did not change much when reaction temperature was <170°C. With reaction temperature >170°C, the gas-phase N<sub>2</sub>O bands (~2210 cm<sup>-1</sup> and ~2240 cm<sup>-1</sup>) were clearly shown in the spectra, partially overlapping with the gas phase CO band. According Cheng et al,<sup>25</sup> the 2210 cm<sup>-1</sup> band was sometimes assigned to -NCO intermediate species. However, the authors found the -NCO band started showing at 150°C and disappeared at 210°C, which is not in agreement with our results. Therefore, it is reasonable to believe that the 2210 cm<sup>-1</sup> band in the current work was from gas phase N<sub>2</sub>O instead of -NCO species. The intensity of the gas-phase N<sub>2</sub>O band increased when temperature increased from 170°C to 180°C, then decreased as the reaction temperature increased further. This result also matched with the N<sub>2</sub>O selectivity from the activity test (Figure 5 (d)), where the N<sub>2</sub>O selectivity of the 5% NiO<sub>x</sub>/CeO<sub>2</sub> catalyst was the highest (~100%) at ~180°C, then gradually decreased as reaction temperature increased. The gas phase CO<sub>2</sub> band (~2350 cm<sup>-1</sup>) started showing at 170°C, and the intensity increased along with the reaction temperature, which is in agreement with the increase in CO conversion as shown in Figure 5 (b).

Based on the *in-situ* DRIFTS and activity results, the NO reduction by CO reaction contained two stages. The first stage was dominated by NO chemisorption, where NO interacted with the catalyst surface to form nitrate (and nitrite) intermediate species (50°C~180°C). In this stage, CO adsorption was hindered by nitrate intermediates. In the second stage (>180°C), gas phase CO interacted with catalyst surface and formed carbonate species. Interaction between CO and surface oxygen could produce CO<sub>2</sub> and oxygen vacancies which enhanced the NO dissociation.<sup>68-70</sup> The dissociated N atom interacted with gas phase (or adsorbed) NO and produced N<sub>2</sub>O, which can further react with CO to produce N<sub>2</sub> and CO<sub>2</sub>. As reaction temperature continued to increase, especially >350°C, the NO reduction by CO reaction performed near stoichiometric ratio and NO and CO conversions both reached ~100%.

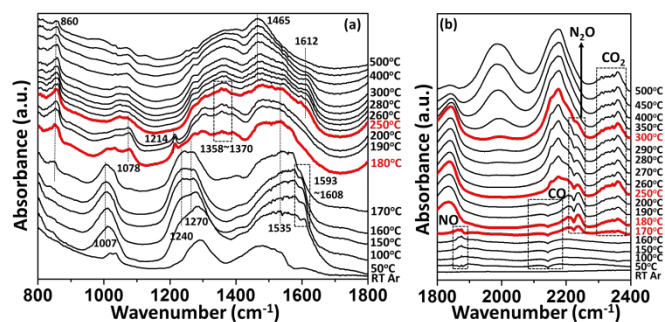


**Figure 9.** In-situ DRIFTS spectra of 5% NiO<sub>x</sub>/CeO<sub>2</sub> catalysts in NO reduction by CO under different reaction temperatures: (a) 800 cm<sup>-1</sup> – 1800 cm<sup>-1</sup> region, and (b) 1800 cm<sup>-1</sup> – 2400 cm<sup>-1</sup> region. Reaction conditions: 5% NO, 5% CO, balanced with Helium. Total flow rate was 40 mL/min.

## Conclusions

In this study, the relationship between structure and catalytic activity of a series of NiO<sub>x</sub>/CeO<sub>2</sub> catalysts (with Ni loading from 0.5 wt% to 30 wt%) in NO reduction by CO reaction was investigated. With increasing Ni loading on the surface of CeO<sub>2</sub>, the specific surface area of the catalysts decreased, in correspondence to the formation of monolayer NiO<sub>x</sub> coverage (4~5 wt% Ni) and NiO crystalline structures (> 6 wt%) confirmed by XRD patterns (Figure 2), Raman spectra (Figure 3) and H<sub>2</sub>-TPR profiles (Figure 4). The synergy effects of NiO<sub>x</sub> and CeO<sub>2</sub> were also noticed in H<sub>2</sub>-TPR results (Figure 4), where in the supported NiO<sub>x</sub>/CeO<sub>2</sub> catalysts, the surface NiO<sub>x</sub> reduction peaks shifted from ~307°C to ~158°C, but did not further decrease after reaching the monolayer coverage of NiO<sub>x</sub> (~5 wt%). The gas phase catalytic activity tests (Figure 5) confirmed that increasing Ni loading after monolayer coverage of NiO<sub>x</sub> did not further improve the NO and CO conversions. The stability test (Figure 7) and space velocity effect tests (Figure 8) of 5% NiO<sub>x</sub>/CeO<sub>2</sub> catalyst displayed the steady performance of the NiO<sub>x</sub>/CeO<sub>2</sub> catalysts under various reaction conditions. *In-situ* DRIFTS results of 5% NiO<sub>x</sub>/CeO<sub>2</sub> catalyst (Figure 9) confirmed the activity results where NO conversion started at ~170°C and reached ~100% at ~185°C. N<sub>2</sub>O selectivity (Figure 5(d)) was confirmed as the gas phase N<sub>2</sub>O band appeared at 170°C and the intensity maximized at 180°C, then decreased as the temperature increased. Furthermore, *in-situ* DRIFTS results indicated a two-stage reaction mechanism in NO reduction by CO reaction over the NiO<sub>x</sub>/CeO<sub>2</sub> catalyst, where the first stage was dominated by NO interacting with the catalyst surface and forming various nitrate/nitrite intermediate species, and the second stage with CO interacting with the catalyst and intermediate species to produce CO<sub>2</sub> as well as N<sub>2</sub>.

## Conflicts of interest

There are no conflicts to declare.

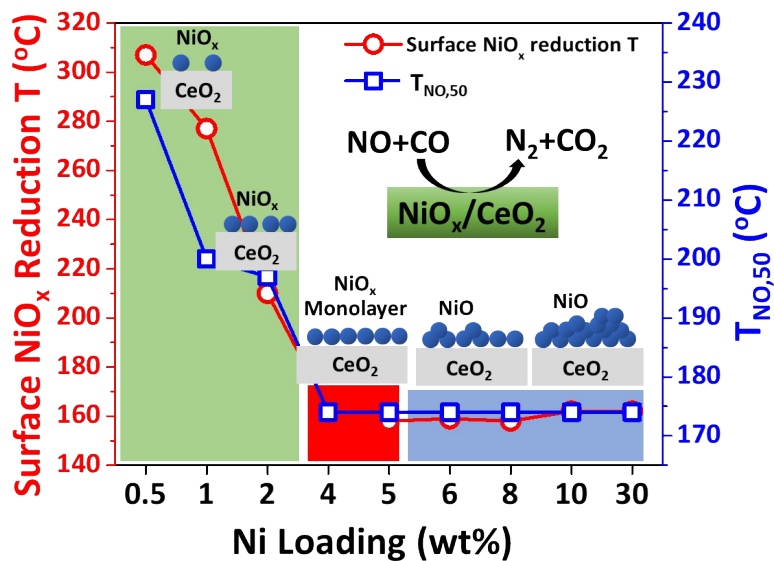
## Acknowledgements

S. Zhang and T. Kim would like to thank the Advanced Energy Research and Technology Center (AERTC) at the Stony Brook University for the facilities. The authors would also like to thank Kyung-Min Lee for his assistance in performing Raman experiments and Katie Wooton for her help in the ICP-MS experiments. This work was also partially supported by the National Research Foundation of Korea (NRF) grant funded by the South Korea government (MSIP) (NRF-2016R1A5A1009592).

## References

- 1 A. L. Karemure, P. D. Vaidya, R. Sinha and P. Chugh, *Int. J. Hydrogen Energy*, 2016, **41**, 22963–22975.
- 2 X. Du, X. Gao, W. Hu, J. Yu, Z. Luo and K. Cen, *J. Phys. Chem. C*, 2014, **118**, 13617–13622.
- 3 X. Li, J. Li, Y. Peng, T. Zhang, S. Liu and J. Hao, *Catal. Sci. Technol.*, 2015, **5**, 4556–4564.
- 4 X. Wang, A. Shi, Y. Duan, J. Wang and M. Shen, *Catal. Sci. Technol.*, 2012, **2**, 1386–1395.
- 5 H. S. Gandhi, G. W. Graham and R. W. McCabe, *J. Catal.*, 2003, **216**, 433–442.
- 6 I. Śmiechowicz, I. Kocemba, J. Rogowski and K. Czupryn, *React. Kinet. Mech. Catal.*, 2018, **124**, 633–649.
- 7 A. S. Ivanova, E. M. Slavinskaya, R. V. Gulyaev, V. I. Zaikovskii, O. A. Stonkus, I. G. Danilova, L. M. Plyasova, I. A. Polukhina and A. I. Boronin, *Appl. Catal. B Environ.*, 2010, **97**, 57–71.
- 8 C. Wang, H. Yin, S. Dai and S. Sun, *Chem. Mater.*, 2010, **22**, 3277–3282.
- 9 X. Liu, M. H. Liu, Y. C. Luo, C. Y. Mou, S. D. Lin, H. Cheng, J. M. Chen, J. F. Lee and T. S. Lin, *J. Am. Chem. Soc.*, 2012, **134**, 10251–10258.
- 10 P. Bera, K. C. Patil, V. Jayaram, G. N. Subbanna and M. S. Hegde, *J. Catal.*, 2000, **196**, 293–301.
- 11 A. Eichler and J. Hafner, *J. Catal.*, 2001, **204**, 118–128.
- 12 D. Qiao, G. Lu, Y. Guo, Y. Wang and Y. Guo, *J. Rare Earths*, 2010, **28**, 742–746.
- 13 X. C. Zheng, X. Y. Wang, X. L. Zhang, S. R. Wang and S. H. Wu, *React. Kinet. Catal. Lett.*, 2006, **88**, 57–63.
- 14 X. Zhang, K. Li, W. Shi, C. Wei, X. Song, S. Yang and Z. Sun, *Nanotechnology*, 2017, **28**, 045602.
- 15 W. Fang, C. Pirez, S. Paul, M. Capron, H. Jobic, F. Dumeignil and L. Jalowiecki-Duhamel, *ChemCatChem*, 2013, **5**, 2207–2216.
- 16 X. Wang, J. A. Rodriguez, J. C. Hanson, D. Gamarra, A. Martínez-Arias and M. Fernández-García, *J. Phys. Chem. B*, 2005, **109**, 19595–19603.
- 17 B. M. Reddy, K. N. Rao and P. Bharali, *Ind. Eng. Chem. Res.*, 2009, **48**, 8478–8486.
- 18 L. Atzori, M. G. Cutrufello, D. Meloni, C. Cannas, D. Gazzoli, R. Monaci, M. F. Sini and E. Rombi, *Catal. Today*, 2018, **299**, 183–192.
- 19 P. V. Snytnikov, M. M. Popova, Y. Men, E. V. Rebrov, G. Kolb, V. Hessel, J. C. Schouten and V. A. Sobyanin, *Appl. Catal. A Gen.*, 2008, **350**, 53–62.
- 20 Y. Li, Q. Fu and M. Flytzani-Stephanopoulos, *Appl. Catal. B Environ.*, 2000, **27**, 179–191.
- 21 V. S. Rudnev, L. M. Tyrina, I. V. Lukiyanchuk, T. P. Yarovaya, I. V. Malyshev, A. Y. Ustinov, P. M. Nedozorov and T. A. Kaidalova, *Surf. Coatings Technol.*, 2011, **206**, 417–424.
- 22 J. Lee, Y. Ryou, J. Kim, X. Chan, T. J. Kim and D. H. Kim, *J. Phys. Chem. C*, 2018, **122**, 4972–4983.
- 23 L. He, B. Liang, L. Li, X. Yang, Y. Huang, A. Wang, X. Wang and T. Zhang, *ACS Catal.*, 2015, **5**, 1623–1628.

- 24 Y. Wang, A. Zhu, Y. Zhang, C. T. Au, X. Yang and C. Shi, *Appl. Catal. B Environ.*, 2008, **81**, 141–149.
- 25 X. Cheng, A. Zhu, Y. Zhang, Y. Wang, C. T. Au and C. Shi, *Appl. Catal. B Environ.*, 2009, **90**, 395–404.
- 26 T. Xu, J. Xue, X. Zhang, G. He and H. Chen, *Appl. Surf. Sci.*, 2017, **402**, 294–300.
- 27 J. Taghavimoghaddam, G. P. Knowles and A. L. Chaffee, *J. Mol. Catal. A Chem.*, 2012, **358**, 79–88.
- 28 N. Srivastava and P. C. Srivastava, *Bull. Mater. Sci.*, 2010, **33**, 653–656.
- 29 Y. H. Liu, J. C. Zuo, X. F. Ren and L. Yong, *Metalurgija*, 2014, **53**, 463–465.
- 30 X. Yin, Y. Zhang, Z. Fang, Z. Xu and W. Zhu, *Nanosci. Methods*, 2012, **1**, 115–122.
- 31 X. Yao, Q. Yu, Z. Ji, Y. Lv, Y. Cao, C. Tang, F. Gao, L. Dong and Y. Chen, *Appl. Catal. B Environ.*, 2013, **130–131**, 293–304.
- 32 X. Yao, Y. Xiong, W. Zou, L. Zhang, S. Wu, X. Dong, F. Gao, Y. Deng, C. Tang, Z. Chen, L. Dong and Y. Chen, *Appl. Catal. B Environ.*, 2014, **144**, 152–165.
- 33 C. Deng, B. Li, L. Dong, F. Zhang, M. Fan, G. Jin, J. Gao, L. Gao, F. Zhang and X. Zhou, *Phys. Chem. Chem. Phys.*, 2015, **17**, 16092–16109.
- 34 C. Deng, M. Li, J. Qian, Q. Hu, M. Huang, Q. Lin, Y. Ruan, L. Dong, B. Li and M. Fan, *Chem. - An Asian J.*, 2016, **11**, 2144–2156.
- 35 T. C. Peck, G. K. Reddy, M. Jones and C. A. Roberts, *J. Phys. Chem. C*, 2017, **121**, 8435–8443.
- 36 S. Zhang, Y. Li, J. Huang, J. Lee, D. H. Kim, A. I. Frenkel and T. Kim, *J. Phys. Chem. C*, 2019, **123**, 7166–7177.
- 37 Q. Xie, H. Zhang, J. Kang, J. Cheng, Q. Zhang and Y. Wang, *ACS Catal.*, 2018, **8**, 4902–4916.
- 38 W. W. Wang, W. Z. Yu, P. P. Du, H. Xu, Z. Jin, R. Si, C. Ma, S. Shi, C. J. Jia and C. H. Yan, *ACS Catal.*, 2017, **7**, 1313–1329.
- 39 W. Zou, L. Liu, L. Zhang, L. Li, Y. Cao, X. Wang, C. Tang, F. Gao and L. Dong, *Appl. Catal. A Gen.*, 2015, **505**, 334–343.
- 40 X. Du, D. Zhang, L. Shi, R. Gao and J. Zhang, *J. Phys. Chem. C*, 2012, **116**, 10009–10016.
- 41 F. T. Thema, E. Manikandan, A. Gurib-Fakim and M. Maaza, *J. Alloys Compd.*, 2016, **657**, 655–661.
- 42 J. Ciro, D. Ramírez, M. A. Mejía Escobar, J. F. Montoya, S. Mesa, R. Betancur and F. Jaramillo, *ACS Appl. Mater. Interfaces*, 2017, **9**, 12348–12354.
- 43 N. Mironova-Ulmane, A. Kuzmin, I. Steins, J. Grabis, I. Sildos and M. Pärs, *J. Phys. Conf. Ser.*, 2007, **93**, 012039.
- 44 R. E. Dietz, G. I. Parisot and A. E. Meixner, *J. Appl. Phys.*, 1971, **42**, 1484.
- 45 M. Gil-Calvo, C. Jiménez-González, B. De Rivas, J. I. Gutiérrez-Ortiz and R. López-Fonseca, *Ind. Eng. Chem. Res.*, 2017, **56**, 6186–6197.
- 46 L. Pino, A. Vita, F. Cipiti, M. Laganà and V. Recupero, *Catal. Letters*, 2008, **122**, 121–130.
- 47 J. J. Wang, M. Shen, J. J. Wang, J. Gao, J. Ma and S. Liu, *Catal. Today*, 2011, **175**, 65–71.
- 48 S. Mahammadunnisa, P. Manoj Kumar Reddy, N. Lingaiah and C. Subrahmanyam, *Catal. Sci. Technol.*, 2013, **3**, 730–736.
- 49 W. Zou, M. Lu, S. Wu, Y. Wang, Y. Pu, C. Tang, F. Gao, L. Dong, J. Sun and C. Ge, *RSC Adv.*, 2015, **5**, 98335–98343.
- 50 J. Y. Luo, M. Meng, J. S. Yao, X. G. Li, Y. Q. Zha, X. Wang and T. Y. Zhang, *Appl. Catal. B Environ.*, 2009, **87**, 92–103.
- 51 N. Acerbi, S. C. E. Tsang, G. Jones, S. Golunski and P. Collier, *Angew. Chemie Int. Ed.*, 2013, **52**, 7737–7741.
- 52 W. Karim, C. Spreafico, A. Kleibert, J. Gobrecht, J. VandeVondele, Y. Ekinici and J. A. van Bokhoven, *Nature*, 2017, **541**, 68–71.
- 53 G. N. Vayssilov, Y. Lykhach, A. Migani, T. Staudt, G. P. Petrova, N. Tsud, T. Skála, A. Bruix, F. Illas and K. C. Prince, *Nat. Mater.*, 2011, **10**, 310–315.
- 54 Y. Lu, C. Thompson, D. Kunwar, A. Datye and A. M. Karim, *ChemCatChem*, 2020, **12**, 1–9. View Article Online  
DOI: 10.1039/C9CY02619C
- 55 Y. Lykhach, A. Figueroba, M. F. Camellone, A. Neitzel, T. Skála, F. R. Negreiros, M. Vorokhta, N. Tsud, K. C. Prince and S. Fabris, *Phys. Chem. Chem. Phys.*, 2016, **18**, 7672–7679.
- 56 C. Tang, B. Sun, J. Sun, X. Hong, Y. Deng, F. Gao and L. Dong, *Catal. Today*, 2017, **281**, 575–582.
- 57 Y. Kim, S. Hwang, J. Lee, Y. Ryou, H. Lee, C. H. Kim and D. H. Kim, *Emiss. Control Sci. Technol.*, 2019, **5**, 172–182.
- 58 L. Xue, C. Zhang, H. He and Y. Teraoka, *Appl. Catal. B Environ.*, 2007, **75**, 167–174.
- 59 L. F. Liotta, G. Pantaleo, G. Di Carlo, G. Marci and G. Deganello, *Appl. Catal. B Environ.*, 2004, **52**, 1–10.
- 60 C. Deng, Q. Huang, X. Zhu, Q. Hu, W. Su, J. Qian, L. Dong, B. Li, M. Fan and C. Liang, *Appl. Surf. Sci.*, 2016, **389**, 1033–1049.
- 61 F. Amano, S. Suzuki, T. Yamamoto and T. Tanaka, *Appl. Catal. B Environ.*, 2006, **64**, 282–289.
- 62 L. Liu, B. Liu, L. Dong, J. Zhu, H. Wan, K. Sun, B. Zhao, H. Zhu, L. Dong and Y. Chen, *Appl. Catal. B Environ.*, 2009, **90**, 578–586.
- 63 X. Dai, W. Jiang, W. Wang, X. Weng, Y. Shang, Y. Xue and Z. Wu, *Cuihua Xuebao/Chinese J. Catal.*, 2018, **39**, 728–735.
- 64 L. Zhang, X. Yao, Y. Lu, C. Sun, C. Tang, F. Gao and L. Dong, *J. Colloid Interface Sci.*, 2018, **509**, 334–345.
- 65 C. Li, Y. Sakata, T. Arai, K. Domen, K. I. Maruya and T. Onishi, *J. Chem. Soc. Faraday Trans. 1 Phys. Chem. Condens. Phases*, 1989, **85**, 1451–1461.
- 66 T. Y. Chen, J. Su, Z. Zhang, C. Cao, X. Wang, R. Si, X. Liu, B. Shi, J. Xu and Y. F. Han, *ACS Catal.*, 2018, **8**, 8606–8617.
- 67 K. I. Hadjiivanov and G. N. Vayssilov, *Adv. Catal.*, 2002, **47**, 307–511.
- 68 X. Yao, L. Li, W. Zou, S. Yu, J. An, H. Li, F. Yang and L. Dong, *Cuihua Xuebao/Chinese J. Catal.*, 2016, **37**, 1369–1380.
- 69 D. Li, Q. Yu, S. S. Li, H. Q. Wan, L. J. Liu, L. Qi, B. Liu, F. Gao, L. Dong and Y. Chen, *Chem. - A Eur. J.*, 2011, **17**, 5668–5679.
- 70 X. Yao, F. Gao, Q. Yu, L. Qi, C. Tang, L. Dong and Y. Chen, *Catal. Sci. Technol.*, 2013, **3**, 1355–1366.



NO reduction by CO reaction was investigated by NiO/CeO<sub>2</sub> catalysts with different Ni loadings. Surface NiO controls the catalytic activity which was related to the molecular structure and reducibility of catalysts.